AIAA 2005-4534

# The Taylor-Culick Profile with Uniform Headwall Injection

Joseph Majdalani
Advanced Theoretical Research Center
University of Tennessee Space Institute
Tullahoma, TN 37388

**41st AIAA/ASME/SAE/ASEE Joint Propulsion Conference and Exhibit**
10–13 July 2005
Tucson, AZ

41st AIAA/ASME/SAE/ASEE Joint Propulsion Conference and Exhibit
10-13 July 2005, Tucson, Arizona

AIAA 2005-4534

# The Taylor-Culick Profile with Uniform Headwall Injection

Joseph Majdalani*
*University of Tennessee Space Institute, Tullahoma, TN 37388*

**Taylor's incompressible and rotational profile is extended to a porous cylinder with uniform headwall injection. This profile, often referred to in the propulsion community as Culick's mean flow, is now generalized to permit the imposition of reactive headwall conditions. Starting with Euler's steady equations, the solution that we derive is exact and quasi-viscous because it observes the no slip condition along both headwall and sidewall. It is ideally suited to describe the bulk flowfield in models of solid and hybrid rockets where uniform surface injection may be assumed. It may also be used to mimic the flowfield in short cylindrical motor segments such as upper stage rockets and T-burners. In closing, our solution is generalized to the extent of accommodating arbitrary headwall injection velocities including those prescribed by conventional laminar and turbulent flow representations.**

## Nomenclature

| | |
|---|---|
| $a$ | = chamber radius |
| $a_0$ | = speed of sound |
| $r$ , $z$ | = normalized radial and axial coordinates, $\bar{r}/a$ , $\bar{z}/a$ |
| $\boldsymbol{u}$ | = normalized velocity $(\bar{u}_r, \bar{u}_z)/U_w$ |
| $U_0$ | = uniform headwall injection velocity, $\bar{u}_z(\bar{r},0)$ |
| $u_0$ | = normalized headwall injection velocity, $U_0/U_w$ |
| $u_h$ | = headwall injection constant, $u_0/\pi = U_0/(\pi U_w)$ |
| $U_w$ | = sidewall injection velocity, $-\bar{u}_r(a,\bar{z})$ |
| $\gamma$ | = ratio of specific heats |
| $\nu$ | = kinematic viscosity, $\mu/\rho$ |
| $\rho$ | = density |

*Subscripts and Symbols*

| | |
|---|---|
| $h$ , $w$ | = property at headwall or sidewall |
| $r$ | = radial component |
| $z$ | = axial (streamwise) component |
| | = overbars denote dimensional variables |

## I. Introduction

CULICK's simple analytical solution for describing the gaseous motion in solid rocket motors (SRMs) was obtained under the contingencies of steady, incompressible, rotational, axisymmetric, and quasi-viscous flow.[1] Despite being inviscid, its streamlines observed the no slip requirement along the porous wall. It also coincided with Taylor's 1956 solution obtained a decade earlier, albeit in an entirely different physical context.[2] The Taylor-Culick profile was repeatedly verified in a reassuring number of investigations, starting with the inventive tests reported by Taylor,[2] and continuing to those carried out in later years by way of computation,[3-5] experiment,[5-7] and theory.[8-10] In short, a collective body of research has confirmed the adequacy of the Taylor-Culick model in approximating the bulk flow in a full-length cylindrical motor.[11] Since then, this profile has stood at the foundation of many theoretical studies, especially, those concerned with wave propagation[12-14] and both hydrodynamic and combustion instability theories in porous chambers with and without particle interactions.[15-26]

*Jack D. Whitfield Professor of High Speed Flows, Department of Mechanical, Aerospace and Biomedical Engineering. Member AIAA.

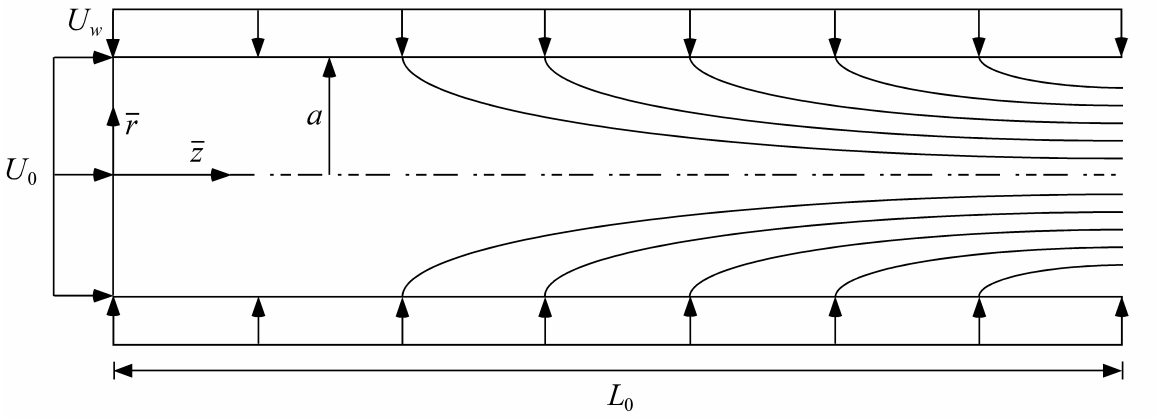


**Figure 1. Simulated rocket chamber as a porous tube with uniform headwall injection.**

Recently, the Taylor-Culick profile has been extended to a simulated motor with regressing walls; this was accomplished using a nozzleless, nonreactive, rotational, viscous, and incompressible approximation that invoked similarity in time to model the expansion pattern of the porous wall.[8] It has also been submitted by Majdalani and Vyas,[27] following a simple modification, as a viable model for simulating the bulk motion in hybrid rockets exhibiting circular-port fuel grains. This was achieved by using a sinusoidal headwall injection profile to mimic oxidizer injection. In this article, we reconstruct the solution for uniform headwall injection to the extent of making it applicable to both solid and hybrid rockets in which the inflow at the headwall is nearly uniform. As one may expect, the headwall-to-sidewall injection velocity ratio will be significantly larger in the case of hybrids, thus leading to the onset of streamtube motion; our solution will attempt to capture this behavior. The ensuing formulation will constitute a basic approximation as it discounts the effects of compressibility, mixing, viscosity, and chemical reactions. However, by satisfying the no slip condition on all walls, we expect it to exhibit a quasi-viscous trait akin to that displayed by the Taylor-Culick solution. The same may be said of the generalized solution that we later pursue with the aim of accommodating arbitrary headwall injection profiles. The attendant analysis will be considered last and shown to represent other possible injection scenarios.

## II. Mathematical Model

As usual, the motor can be idealized as a cylindrical chamber of porous length $L_0$ and radius $a$ with both a 'reactive' headwall and a nozzleless aft end (see Fig. 1). At the headwall, a fluid stream (which may denote an oxidizer or gaseous propellant mixture) is injected into the chamber at an axially uniform speed $U_0$. This incoming stream must be assimilated with the lateral crossflow sustained by uniform mass addition along the porous sidewall. Naturally, the sidewall injection velocity $U_w$ is commensurate with the solid propellant or fuel regression rates. In hybrids, $U_w$ can be appreciably smaller than $U_0$ due to slow fuel pyrolysis, whereas these two values will be the same in SRM analysis. As shown in Fig. 1, $\bar{r}$ and $\bar{z}$ stay for the radial and axial coordinates used to describe the solution from the headwall to the typical nozzle attachment point at the aft end.

### A. Normalization

For expediency, it is helpful to begin by normalizing all recurring variables and operators. This can be done by setting, as before,[27]

$$z = \frac{\bar{z}}{a};\ r = \frac{\bar{r}}{a};\ \nabla = a\bar{\nabla};\ p = \frac{\bar{p}}{\rho U_w^2};\ \psi = \frac{\bar{\psi}}{a^2 U_w} \tag{1}$$

$$u_r = \frac{\bar{u}_r}{U_w};\ u_z = \frac{\bar{u}_z}{U_w};\ \boldsymbol{\Omega} = \frac{\bar{\boldsymbol{\Omega}} a}{U_w};\ u_0 = \frac{U_0}{U_w};\ L = \frac{L_0}{a} \tag{2}$$

Here $U_0 = \bar{u}_z(0,0)$ and $U_w = -\bar{u}_r(a,\bar{z})$ allude to the uniform fluid injection velocities along the headwall and sidewall, respectively. For steady inviscid motion, the vorticity transport equation reduces to

$$\nabla \times \boldsymbol{u} \times \boldsymbol{\Omega} = 0\ ;\quad \boldsymbol{\Omega} = \nabla \times \boldsymbol{u} \tag{3}$$

An assortment of four boundary conditions can be prescribed, as usual, by writing[27]

$$\begin{cases} u_r(0,z) = 0 \text{ (no flow across centerline)} \\ u_z(1,z) = 0 \text{ (no slip at sidewall)} \\ u_r(1,z) = -1 \text{ (constant radial inflow at sidewall)} \\ u_z(r,0) = u_0 \text{ (axial inflow at headwall)} \end{cases} \tag{4}$$

**B. Vorticity-Stream Function Approach**

Continuity is fulfilled by the Stokes stream function when it is defined by

$$u_r = -\frac{1}{r}\frac{\partial \psi}{\partial z} \qquad u_z = \frac{1}{r}\frac{\partial \psi}{\partial r} \tag{5}$$

Substitution into Eq. (3) requires

$$\Omega = \Omega_\theta = rF(\psi) \tag{6}$$

So we follow tradition[1] and select

$$\Omega = C^2 r\psi \tag{7}$$

Despite the non-uniqueness of this relation, we will later show that it allows us to fully satisfy Eq. (4). Straightforward substitution into the vorticity equation yields the standard PDE, namely,

$$\frac{\partial^2 \psi}{\partial z^2} + \frac{\partial^2 \psi}{\partial r^2} - \frac{1}{r}\frac{\partial \psi}{\partial r} + C^2 r^2 \psi = 0 \tag{8}$$

with the particular set of constraints:

$$\lim_{r\to 0} \frac{1}{r}\frac{\partial \psi(r,z)}{\partial z} = 0 \quad \text{(a)}; \quad \frac{\partial \psi(1,z)}{\partial r} = 0 \quad \text{(b)}; \quad \frac{1}{r}\frac{\partial \psi(1,z)}{\partial z} = 1 \quad \text{(c)}; \quad \frac{1}{r}\frac{\partial \psi(r,0)}{\partial r} = u_0 \quad \text{(d)} \tag{9}$$

By virtue of L'Hôpital's rule, removing the singularity in Eq. (9)a requires that both

$$\frac{\partial \psi(0,z)}{\partial z} = 0 \quad \text{(a)} \qquad \text{and} \qquad \frac{\partial^2 \psi(0,z)}{\partial r \partial z} = 0 \quad \text{(b)} \tag{10}$$

Equation (8) is readily solved by separation of variables; one finds

$$\psi(r,z) = (\alpha z + \beta)[A\cos(\tfrac{1}{2}Cr^2) + B\sin(\tfrac{1}{2}Cr^2)] \tag{11}$$

This expression satisfies Eq. (10)b identically. Thus, from this point forward, Eq. (9)a may be superseded by Eq. (10)a.

## III. Solutions

**A. Solution by General Eigenfunction Expansions**

Application of the boundary conditions must be carefully carried out, preferably, in the order in which they appear. For example, Eq. (10)a gives:

$$\frac{\partial \psi(0,z)}{\partial z} = \alpha A\cos(\tfrac{1}{2}Cr^2) + \alpha B\sin(\tfrac{1}{2}Cr^2)\Big|_{r=0} = 0 \tag{12}$$

or $A = 0$. Without loss in generality, we set $B = 1$ and rewrite Eq. (9)b as

$$rC(\alpha z + \beta)\cos(\tfrac{1}{2}Cr^2)\Big|_{r=1} = 0; \quad \forall z \tag{13}$$

and so $\cos(\frac{1}{2}C) = 0$; this is satisfied by

$$C = C_n = (2n+1)\pi;\ n = \{0,1,2,...,\infty\} \in \mathbb{N} \tag{14}$$

Using $C_n = (2n+1)\pi$ enables us to sum over eigenfunctions corresponding to wall suction and injection. When even integers are considered, only injection-driven eigenfunctions will be employed. We now put

$$\psi_n(r,z) = (\alpha_n z + \beta_n)\sin[(n+\tfrac{1}{2})\pi r^2] \text{ or } \psi(r,z) = \sum_{n=0}^{\infty}(\alpha_n z + \beta_n)\sin[(n+\tfrac{1}{2})\pi r^2] \tag{15}$$

The third condition becomes

$$\frac{\partial \psi(1,z)}{\partial z} = \sum_{n=0}^{\infty}\alpha_n \sin[(n+\tfrac{1}{2})\pi] = 1 \text{ or } \sum_{n=0}^{\infty}(-1)^n\alpha_n = 1 \tag{16}$$

which may exhibit several outcomes depending on the behavior of $\alpha_n$. Finally, the headwall condition may be satisfied by evoking the ideas of superposition and orthogonality. Starting with

$$\frac{1}{r}\frac{\partial \psi(r,0)}{\partial r} = \pi \sum_{n=0}^{\infty} (2n+1)\beta_n \cos[(n+\tfrac{1}{2})\pi r^2] = u_0 \tag{17}$$

one can apply orthogonality to secure

$$\beta_n \int_0^1 (2n+1)\cos^2[(n+\tfrac{1}{2})\pi r^2]\, r\, \mathrm{d}r = \frac{u_0}{\pi}\int_0^1 \cos[(n+\tfrac{1}{2})\pi r^2]\, r\, \mathrm{d}r \tag{18}$$

or

$$\beta_n = \frac{4(-1)^n}{\pi^2(2n+1)^2}\frac{U_0}{U_w} = \frac{4(-1)^n u_0}{\pi^2(2n+1)^2} = \frac{4(-1)^n u_h}{\pi(2n+1)^2} \tag{19}$$

Backward substitution into Eq. (15) enables us to extract

$$\psi(r,z) = \sum_{n=0}^{\infty}(-1)^n \left[\alpha_n z + \frac{4u_0}{\pi^2(2n+1)^2}\right]\sin[(n+\tfrac{1}{2})\pi r^2] \tag{20}$$

Note that many solutions may be arrived at depending on the choice of $\alpha_n$ that properly fulfills Eq. (16). One such case corresponds to Taylor's classic solution for which

$$\alpha_0 = 1 \text{ and } \alpha_n = 0; \forall n \neq 0 \tag{21}$$

At the outset, Eq. (20) reduces to

$$\psi(r,z) = z\sin(\tfrac{1}{2}\pi r^2) + \frac{4u_0}{\pi^2}\sum_{n=0}^{\infty}\frac{(-1)^n}{(2n+1)^2}\sin[(n+\tfrac{1}{2})\pi r^2] \tag{22}$$

This expression is deliberately left as an infinite series albeit collapsible into closed form when put in terms of special functions. The character of Eq. (22) is illustrated in Fig. 2 for a headwall injection rate appropriate of SRMs with reactive headend (or T-burners). Using $u_0 = 1$, a balance between sidewall and headwall injection causes the

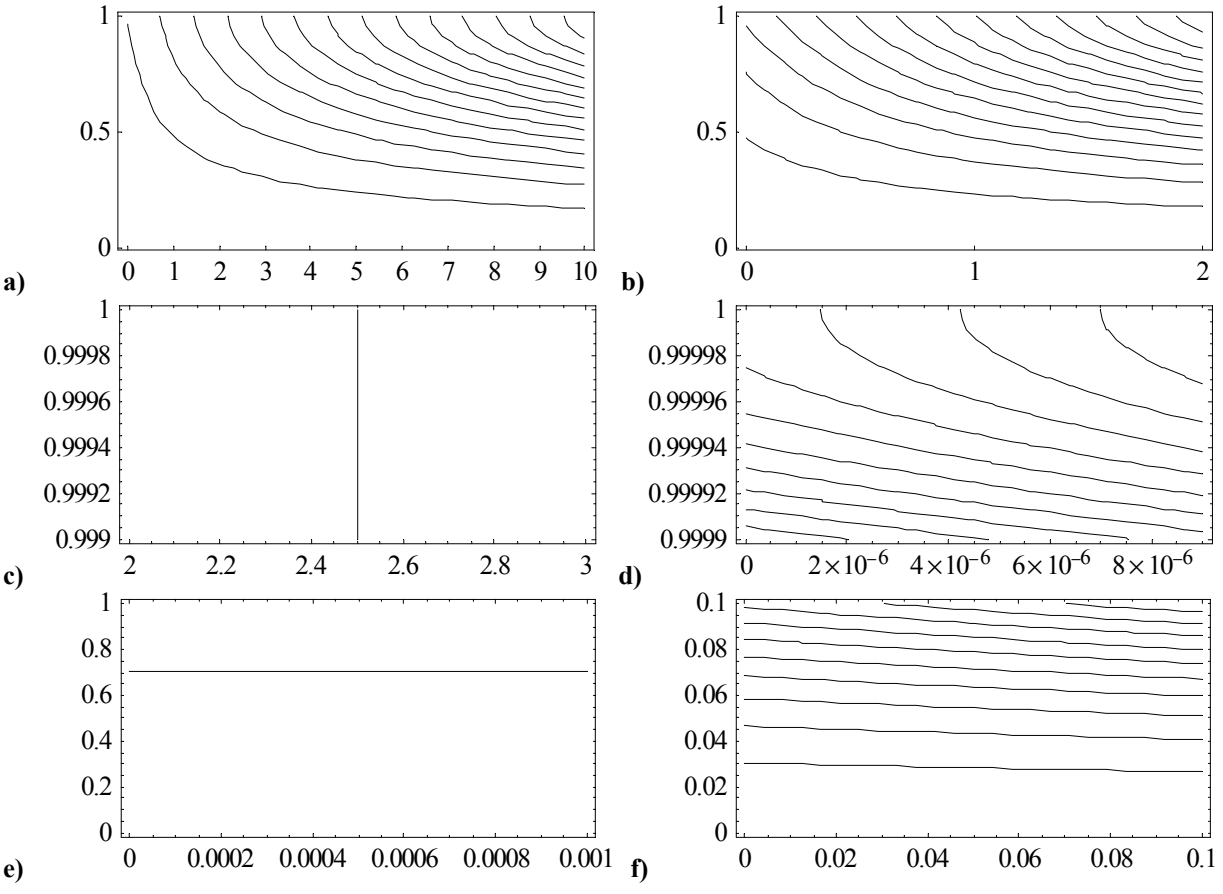


**Figure 2. Streamlines for $u_0$ = 1 depicted in the $r$–$z$ plane. Results shown in a) through f) are enhancements that illustrate the streamline curvature in different localities.**

streamline originating at the corner (1,0) to bisect the flowfield at an angle of $\frac{1}{4}\pi$. By concentrating on specific areas, it may be seen that the solution conforms to the stated boundary conditions. While Fig. 2b illustrates the corner streamlines, Figs. 2c–f confirm the satisfaction of the no slip condition by reproducing the local behavior in different sectors.

When the same analysis is repeated in Fig. 3 for $u_0 = 1000$, a streamtube motion akin to that of hybrid rocket core flow is seen to dominate. This is true everywhere except in the close vicinity of the sidewall. While Fig. 3a offers an overview of the streamtube motion, magnification near the sidewalls enables us to reaffirm that the fluid enters the chamber perpendicularly to the sidewall. By approaching the headwall, the presence of parallel flow in Figs. 3e–f lends support to the local orthogonality.

Having determined $\psi$, the velocity and vorticity components may be recovered from Eqs. (5) and (7). One obtains

$$\begin{cases} u_r(r) = -r^{-1}\sin(\frac{1}{2}\pi r^2) \qquad u_z(r,z) = \pi z\cos(\frac{1}{2}\pi r^2) + \dfrac{4u_0}{\pi}\displaystyle\sum_{n=0}^{\infty}\frac{(-1)^n}{(2n+1)}\cos[(n+\tfrac{1}{2})\pi r^2] \\ \Omega(r,z) = \pi^2 rz\sin(\frac{1}{2}\pi r^2) \end{cases} \tag{23}$$

Note that uniform headwall injection does not introduce any mean flow vorticity and that $u_z(1,z) = 0$ because each $\cos[(n+\frac{1}{2})\pi]$ term vanishes along the sidewall. This behavior is illustrated in Figs. 4a and 4b at the headwall and, using $L = 2$, at six equally-spaced axial stations corresponding to 0, 0.4, 0.8, 1.2, 1.6 and 2. It may be interesting to note that the streamwise velocity is also collapsible into closed form by recognizing that

$$\frac{4u_0}{\pi}\sum_{n=0}^{\infty}\frac{(-1)^n}{(2n+1)}\cos[(n+\tfrac{1}{2})\pi r^2] = \frac{2u_0}{\pi}q(r) = u_0\left[1-\delta_k(1-r)\right] \tag{24}$$

where $\delta_k$ is the Kronecker delta and $q(r) = \tan^{-1}(e^{\frac{1}{2}i\pi r^2}) + \tan^{-1}(e^{-\frac{1}{2}i\pi r^2})$.

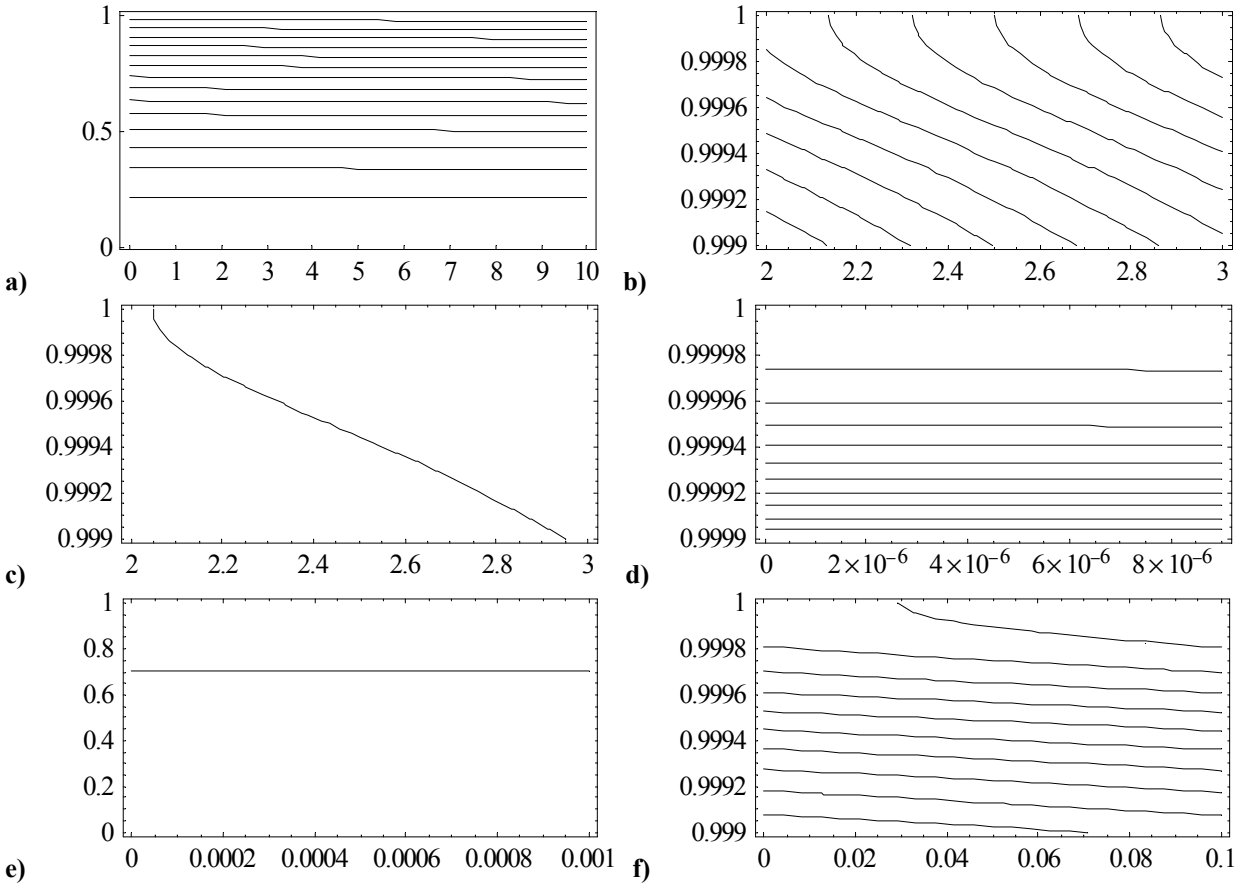


**Figure 3. Same as previous except for $u_0 = 1000$.**

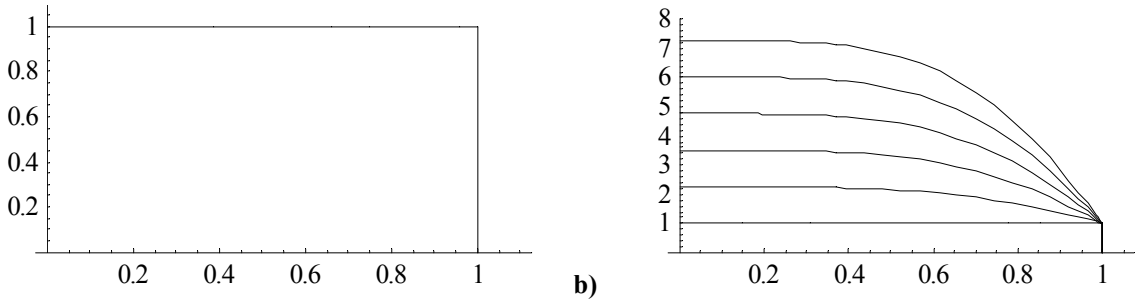


**Figure 4. Radial evolution of the streamwise velocity corresponding to $u_0 = 1$ for a simulated SRM with reactive headwall. Results are shown at a) $z = 0$ and b) six equidistant positions corresponding to $z = 0, 0.4, 0.8, 1.2, 1.6$ and 2.**

### B. Solution by Injection-Driven Eigenfunctions

The same analysis may be repeated by retaining only the even eigenvalues associated with an injection-driven wall contribution. This can be seen by reconsidering Eq. (13) and writing

$$C = C_n = (4n+1)\pi;\ n \in \mathbb{Z} \tag{25}$$

This choice enables us to skip every other multiple of $\frac{1}{2}\pi$, thus producing a series of injection-based solutions. At the outset, the third condition becomes

$$\sum_{n=-\infty}^{\infty} \alpha_n \sin[(2n+\tfrac{1}{2})\pi] = 1 \quad \text{or} \quad \sum_{n=-\infty}^{\infty} \alpha_n = 1 \tag{26}$$

Note that we start our sum at negative infinity lest we capture half of the headwall injection velocity. As we pursue this route, the headwall requirement reduces to

$$\pi \sum_{n=-\infty}^{\infty} (4n+1)\beta_n \cos[(2n+\tfrac{1}{2})\pi r^2] = u_0 \tag{27}$$

and so, by use of orthogonality, we put

$$\beta_n \int_0^1 (4n+1)\cos^2[(2n+\tfrac{1}{2})\pi r^2]\, r\, \mathrm{d}r = \frac{u_0}{\pi}\int_0^1 \cos[(2n+\tfrac{1}{2})\pi r^2]\, r\, \mathrm{d}r \tag{28}$$

with the direct result of

$$\beta_n = \frac{4u_0}{\pi^2(4n+1)^2} = \frac{4u_h}{\pi(4n+1)^2} \tag{29}$$

The injection-based streamfunction becomes

$$\psi_{inj}(r,z) = \sum_{n=-\infty}^{\infty}\left[\alpha_n z + \frac{4u_0}{\pi^2(4n+1)^2}\right]\sin[(2n+\tfrac{1}{2})\pi r^2] \tag{30}$$

Note that both $\psi_{inj}$ and $\psi$ represent exact solutions for this problem. A special case of Eq. (30) corresponds to $\alpha_0 = 1$ and $\alpha_n = 0; \forall n \neq 0$. The injection-driven solution becomes

$$\psi_{inj}(r,z) = z\sin(\tfrac{1}{2}\pi r^2) + \frac{4u_0}{\pi^2}\sum_{n=-\infty}^{\infty}(4n+1)^{-2}\sin[(2n+\tfrac{1}{2})\pi r^2] \tag{31}$$

Although bearing a slightly different look, Eq. (31) is identical to Eq. (22). The seemingly dissimilar part corresponds to the streamwise velocity which can be readily identified as

$$u_z(r,z) = \pi z\cos(\tfrac{1}{2}\pi r^2) + \frac{4u_0}{\pi}\sum_{n=-\infty}^{\infty}\frac{1}{(4n+1)}\cos[(2n+\tfrac{1}{2})\pi r^2] \tag{32}$$

This result merely duplicates the behavior of Eq. (23) especially that, at $r = 0$, one may use the convergent series

$$\sum_{n=-\infty}^{\infty}\frac{1}{(4n+1)} = \frac{\pi}{4} \tag{33}$$

to write $u_z(0,z) = \pi z + u_0$. Similarly, at the sidewall, no slip is observed by virtue of $\cos[(2n+\tfrac{1}{2})\pi] = 0, \forall n \in \mathbb{Z}$. In hindsight, had we limited our sum to $n \in \mathbb{N}$, the orthogonality condition would have yielded half of the headwall contribution, namely, $u_z(r,0) = \frac{1}{2}u_0$ and $u_z(0,z) = \pi z + \frac{1}{2}u_0$, which are, of course, inconsistent.

**C. Pressure Analysis**

The steady momentum equation may be readily solved for the pressure distribution. By ignoring the viscous diffusion of vorticity, one may start with $\boldsymbol{u}\cdot\nabla\boldsymbol{u} = -\nabla p$ and integrate in two spatial directions to retrieve, at length,

$$p = p_0 - \tfrac{1}{2}\boldsymbol{u}\cdot\boldsymbol{u} - \int u_r \frac{\partial u_z}{\partial r}\,\mathrm{d}z \tag{34}$$

where $p_0 = p(0,0)$ represents the headwall pressure. Immediate integration and substitution based on Eq. (23) lead to

$$\begin{aligned} p &= p_0 - \tfrac{1}{2}\pi^2 z^2 - \tfrac{1}{2} r^{-2}\sin^2(\tfrac{1}{2}\pi r^2) + \tfrac{1}{2}u_0^2 - 2\pi^{-2}u_0 q(r)\left[u_0 q(r) + \pi^2 z\cos(\tfrac{1}{2}\pi r^2)\right] \\ &= p_0 - \tfrac{1}{2}\pi^2 z^2 - \tfrac{1}{2} r^{-2}\sin^2(\tfrac{1}{2}\pi r^2) + \tfrac{1}{2}u_0^2\delta_k(1-r) - \pi u_0 z\cos(\tfrac{1}{2}\pi r^2)\left[1-\delta_k(1-r)\right] \end{aligned} \tag{35}$$

At the centerline, we recover $p(0,z) = p_0 - \tfrac{1}{2}\pi^2 z^2 - \pi u_0 z$. To put this in Culick's traditional form, we first write the dimensional pressure, $\overline{p} = \overline{p}_0 - \tfrac{1}{2}\rho U_w^2 \pi z(\pi z + 2u_0)$, and then re-normalize by $\overline{p}_0 = \rho a_0^2/\gamma$. Forthwith, we get

$$\begin{aligned} p^* = \overline{p}/\overline{p}_0 &= 1 - \tfrac{1}{2}\gamma M_w^2\left\{\pi^2 z^2 + r^{-2}\sin^2(\tfrac{1}{2}\pi r^2) - u_0^2 + 4\pi^{-2}u_0 q(r)\left[u_0 q(r) + \pi^2 z\cos(\tfrac{1}{2}\pi r^2)\right]\right\} \\ &= 1 - \tfrac{1}{2}\gamma M_w^2\left\{\pi^2 z^2 + r^{-2}\sin^2(\tfrac{1}{2}\pi r^2) - u_0^2\delta_k(1-r) + 2\pi u_0 z\cos(\tfrac{1}{2}\pi r^2)\left[1-\delta_k(1-r)\right]\right\} \end{aligned} \tag{36}$$

with $p^*(0,z) = 1 - \tfrac{1}{2}\gamma M_w^2 \pi z(\pi z + 2u_0)$.

**D. Arbitrary Headwall Injection Profile**

The analysis may be repeated using an arbitrary headwall injection profile. To be specific, one may use

$$u_0(r) = \begin{cases} u_0\cos(\tfrac{1}{2}\pi r^2) & \text{(a)} \\ u_0(1-r^m) & \text{(b)} \\ u_0(1-r)^{1/m} & \text{(c)} \end{cases} \tag{37}$$

These are prescribed by classic profiles used by Berman, Poiseuille, Darcy, and others. For uniform headwall injection, it is evident that $u_0 = 1$ will correspond to a simulated solid propellant grain that is burning evenly along its surfaces. However, when the headwall injection profile is altered according to Eq. (37), the equivalent injection velocity constant needed to produce the same flux at $z = 0$ may be calculated from a simple mass balance, namely,

$$2\int_0^1 u_0(r) r\,\mathrm{d}r = 1 \quad \text{or} \quad u_0 = \begin{cases} \tfrac{1}{2}\pi & \text{(a)} \\ (m+2)/m & \text{(b)} \\ (m+1)(m+\tfrac{1}{2})/m^2 & \text{(c)} \end{cases} \tag{38}$$

In all cases, one may obtain the solution from

$$\psi = z\sin(\tfrac{1}{2}\pi r^2) + \sum_{n=0}^{\infty}\beta_n \sin[(n+\tfrac{1}{2})\pi r^2] \quad \text{and} \quad u_z = \pi z\cos(\tfrac{1}{2}\pi r^2) + \pi\sum_{n=0}^{\infty}(2n+1)\beta_n\cos[(n+\tfrac{1}{2})\pi r^2] \tag{39}$$

As before, orthogonality may be applied to calculate $\beta_n$. We find

$$\beta_n = \frac{\int_0^1 u_0(r)\cos[(n+\tfrac{1}{2})\pi r^2]\, r\,\mathrm{d}r}{\pi\int_0^1 (2n+1)\cos^2[(n+\tfrac{1}{2})\pi r^2]\, r\,\mathrm{d}r} \tag{40}$$

Then using Berman's half-cosine, Eq. (40) may be evaluated to give $\beta_0 = u_0/\pi$ and $\beta_n = 0, n \neq 0$. Equation (39) becomes

$$u_z = \pi z\cos(\tfrac{1}{2}\pi r^2) + u_0\cos(\tfrac{1}{2}\pi r^2) = \pi(z + u_h)\cos(\tfrac{1}{2}\pi r^2) \tag{41}$$

This matches the solution proposed by Majdalani and Vyas[27] for modeling hybrid rocket core flow.

For the Poiseuille profile, one may use $u_0(r) = u_0(1-r^2)$ and extract

$$\beta_n = 8u_0/\lambda_n^3; \quad \lambda_n \equiv \pi + 2n\pi \tag{42}$$

Both Berman's and Poiseuille's headwall injection velocities are illustrated in Fig. 5 using the same representative parameters of Fig. 4 and fixed $u_0 = 1$. As evidenced by the right-hand-side graphs, the effect of varying the headwall injection profile becomes negligible as the chamber length is increased. However, it remains important near the headwall and, therefore, in short chambers such as upper stage SRMs and T-burners. As for the turbulent profiles corresponding to Eq. (37)b, three commonly examined cases may be connected with $m = 6, 8, 10$. These lead to

$$\frac{\lambda_n^{2+m/2}\beta_n}{u_0}=\begin{cases}96\left[(-1)^n\lambda_n-2\right] & m=6\\ 192(-1)^n(\lambda_n^2-8) & m=8\\ 320\left[(-1)^n\lambda_n(\lambda_n^2-24)+48\right] & m=10\end{cases}\quad\text{where}\quad u_0=\begin{cases}4/3 & m=6\\ 5/4 & m=8\\ 6/5 & m=10\end{cases}\ \text{(SRM)}\tag{43}$$

Finally, for the turbulent model associated with Eq. (37)c, one may obtain a recursive relation in terms of the generalized hypergeometric function ${}_pF_q(a;b;z)$; this is

$$\beta_n=\frac{4m^2u_0}{(1+m)(1+2m)\lambda_n}\,{}_pF_q\left(\left\{\tfrac{3}{4},1,\tfrac{5}{4}\right\},\left\{\tfrac{3}{4}+\tfrac{1}{4m},1+\tfrac{1}{4m},\tfrac{5}{4}+\tfrac{1}{4m},\tfrac{3}{2}+\tfrac{1}{4m}\right\},-\tfrac{1}{16}\lambda_n^2\right);\quad u_0=\begin{cases}91/72 & m=6\\ 60/49 & m=7\\ 153/128 & m=8\end{cases}\ \text{(SRM)}\tag{44}$$

The commonly employed (middle) values in Eqs. (43) and (44) are illustrated in Figs. 5e–h using a fixed $u_0=1$.

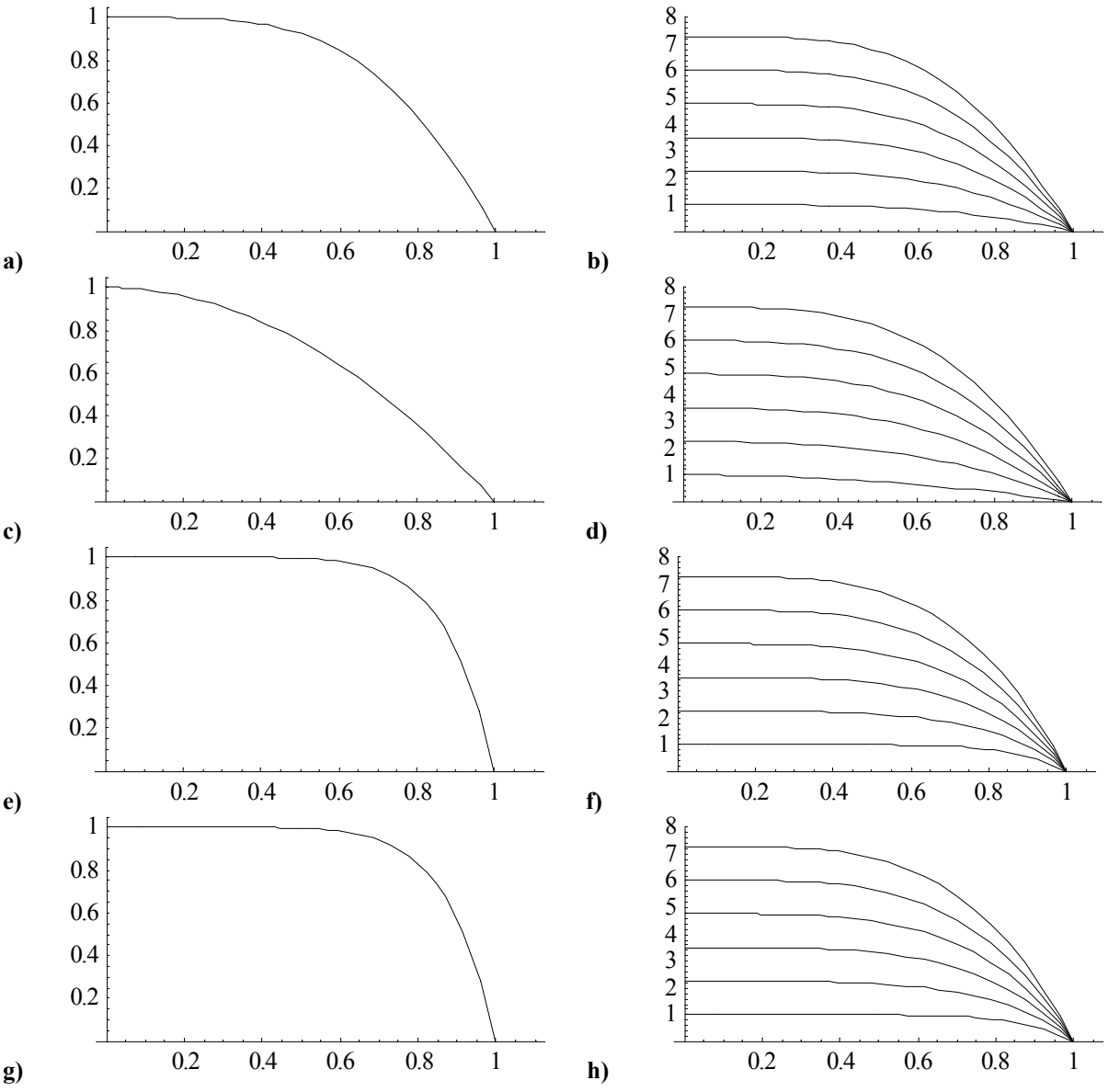


**Figure 5. Radial evolution of the streamwise velocity for $u_0$ = 1 and several headwall inlet profiles associated with a–b) Berman's half-cosine, c–d) Poiseuille, $1-r^2$, e–f) $1-r^8$, and g–h) $(1-r)^{1/7}$. As in Fig. 4, results are shown at the headwall (left) and six equidistant positions corresponding to $z$ = 0, 0.4, 0.8, 1.2, 1.6 and 2 (right).**

### E. A Non-Series Approximation

According to Prandtl's boundary layer theory, the no slip condition at the sidewall need not be satisfied by a standard outer solution due to the absence of friction. If we were to relax this constraint by permitting the streamwise velocity to be finite at the sidewall, the solution will, of course, relinquish its quasi-viscous character. Under these auspices, a simple solution may be obtained in the form of an outer approximation that would later demand a boundary layer treatment along the sidewall. Bearing this in mind, we may choose to ignore the second boundary condition in Eq. (4) and only require that

$$\begin{cases} u_r(0,z) = 0 \\ u_r(1,z) = -1 \\ u_z(r,0) = u_0 \end{cases} \tag{45}$$

In searching for an exact outer solution, we may follow Terrill[28] and superimpose on Taylor's profile (with impervious headwall) a uniform field of zero dimensionality. The resultant is $\psi = \psi_0 + \psi_w$ where $\psi_w = z\sin(\frac{1}{2}\pi r^2)$ is the sidewall-driven Taylor-Culick streamfunction. At the headwall, one may introduce a uniform, axially independent plug flow exhibiting the classic form $\psi_0 = \frac{1}{2}u_0 r^2$ with $u = u_z = u_0$. Note that $\psi_0$ represents a plain irrotational field that still satisfies the vorticity equation by substitution of $C = 0$ in Eq. (8). It also observes three of the original boundary conditions. Overall, $\psi_0$ and $\psi_w$ satisfy, respectively,

$$\begin{cases} u_r(0,z) = 0 \\ u_r(1,z) = 0 \\ u_z(r,0) = u_0 \end{cases} \quad \text{and} \quad \begin{cases} u_r(0,z) = 0 \\ u_r(1,z) = -1 \\ u_z(r,0) = 0 \end{cases} \tag{46}$$

Note that the sum of the separate boundary conditions reproduces Eq. (45). Due to linearity, the composite solution will hence observe the chief requirements, albeit at the expense of carrying $u_z(1,z) = u_0, \forall z$. The composite outer solution is hence expressible by

$$\psi = \tfrac{1}{2}u_0 r^2 + z\sin(\tfrac{1}{2}\pi r^2) \quad u_r(r) = -r^{-1}\sin(\tfrac{1}{2}\pi r^2) \quad u_z(r,z) = u_0 + \pi z\cos(\tfrac{1}{2}\pi r^2) \quad \Omega(r,z) = \pi^2 rz\sin(\tfrac{1}{2}\pi r^2) \tag{47}$$

Equation (47) is similar to Eq. (23) except for the inability to vanish at the sidewall. A viscous boundary layer treatment must be deferred to later work.

## IV. Conclusions

In this study we derive solutions for the incompressible Taylor-Culick flow analogue with uniform headwall injection. Overall, two quasi-viscous solutions are obtained that satisfy all surface requirements including the velocity adherence condition on both headwall and sidewall. These are found to yield identical results. Their behavior is illustrated for the cases of small and large headwall injection in SRM and hybrid rocket models. Our analysis is also extended to account for arbitrary inlet velocity. We find the effect of varying the headwall injection profile to be small in sufficiently long chambers. However, it plays a key role in short rockets and T-burners where the present solutions may be readily used. In hybrid rockets, our models are seen to capture the streamtube motion appropriately. In future work, we hope to explore the existence of other possible solutions with varying types of kinetic energies and viable headwall and sidewall profiles. After securing some exact solutions for this problem, a plain, composite, outer representation is briefly considered and shown to capture the bulk fluid motion away from the sidewall. To satisfy no slip, a boundary layer treatment is mandated and this too is relegated to a forthcoming study. The solutions we obtain increase our collection of engineering approximations that may be used in the modeling of injection-driven porous tubes, particularly, those representing the internal gas dynamics in solid and hybrid rockets.

## Acknowledgments

This work is sponsored by the National Science Foundation through Grant No. CMS-0353518, Program Manager, Dr. Masayoshi Tomizuka. The author acknowledges valuable discussions with Dr. G. Casalis, Professor and Director of the Doctoral School of Aeronautics and Astronautics, SUPAERO, and Research Director, Department of Aerodynamics and Energetics, ONERA, Toulouse, France. His interest in the present work is greatly appreciated. Dr. A. B. Vyas, Visiting Professor at the University of Delaware, is thanked for proposing the other feasible alternative of summing over even integers. The idea of appending uniform headwall injection to Culick's model was first suggested to the author by Dr. G. A. Flandro in 1995.

## References


[1]Culick, F. E. C., "Rotational Axisymmetric Mean Flow and Damping of Acoustic Waves in a Solid Propellant Rocket," *AIAA Journal,* Vol. 4, No. 8, 1966, pp. 1462-1464.

[2]Taylor, G. I., "Fluid Flow in Regions Bounded by Porous Surfaces," *Proceedings of the Royal Society, London, Series A,* Vol. 234, No. 1199, 1956, pp. 456-475.

[3]Baum, J. D., Levine, J. N., and Lovine, R. L., "Pulsed Instabilities in Rocket Motors: A Comparison between Predictions and Experiments," *Journal of Propulsion and Power,* Vol. 4, No. 4, 1988, pp. 308-316.

[4]Sabnis, J. S., Gibeling, H. J., and McDonald, H., "Navier-Stokes Analysis of Solid Propellant Rocket Motor Internal Flows," *Journal of Propulsion and Power,* Vol. 5, No. 6, 1989, pp. 657-664.

[5]Dunlap, R., Willoughby, P. G., and Hermsen, R. W., "Flowfield in the Combustion Chamber of a Solid Propellant Rocket Motor," *AIAA Journal,* Vol. 12, No. 10, 1974, pp. 1440-1445.

[6]Dunlap, R., Blackner, A. M., Waugh, R. C., Brown, R. S., and Willoughby, P. G., "Internal Flow Field Studies in a Simulated Cylindrical Port Rocket Chamber," *Journal of Propulsion and Power,* Vol. 6, No. 6, 1990, pp. 690-704.

[7]Yamada, K., Goto, M., and Ishikawa, N., "Simulative Study of the Erosive Burning of Solid Rocket Motors," *AIAA Journal,* Vol. 14, No. 9, 1976, pp. 1170-1176.

[8]Majdalani, J., Vyas, A. B., and Flandro, G. A., "Higher Mean-Flow Approximation for a Solid Rocket Motor with Radially Regressing Walls," *AIAA Journal,* Vol. 40, No. 9, 2002, pp. 1780-1788.

[9]Zhou, C., and Majdalani, J., "Inner and Outer Solutions for the Injection Driven Channel Flow with Retractable Walls," AIAA Paper 2003-3728, June 2003.

[10]Zhou, C., and Majdalani, J., "Improved Mean Flow Solution for Slab Rocket Motors with Regressing Walls," *Journal of Propulsion and Power,* Vol. 18, No. 3, 2002, pp. 703-711.

[11]Apte, S., and Yang, V., "Effect of Acoustic Oscillation on Flow Development in a Simulated Nozzleless Rocket Motor," *Solid Propellant Chemistry, Combustion, and Motor Interior Ballistics*, Vol. 185, edited by V. Yang, T. B. Brill, and W.-Z. Ren, AIAA Progress in Astronautics and Aeronautics, Washington, DC, 2000, pp. 791-822.

[12]Majdalani, J., and Flandro, G. A., "The Oscillatory Pipe Flow with Arbitrary Wall Injection," *Proceedings of the Royal Society, Series A,* Vol. 458, No. 2022, 2002, pp. 1621-1651.

[13]Flandro, G. A., "On Flow Turning," AIAA Paper 95-2530, July 1995.

[14]Flandro, G. A., "Effects of Vorticity Transport on Axial Acoustic Waves in a Solid Propellant Rocket Chamber," *Combustion Instabilities Driven by Thermo-Chemical Acoustic Sources*, Vol. NCA 4, HTD 128, American Society of Mechanical Engineers, New York, 1989, pp. 53-61.

[15]Abu-Irshaid, E. M., Majdalani, J., and Casalis, G., "Stability of Rockets with Headwall Injection," AIAA Paper 2005-3543, July 2005.

[16]Avalon, G., Casalis, G., and Griffond, J., "Flow Instabilities and Acoustic Resonance of Channels with Wall Injection," AIAA Paper 98-3218, July 1998.

[17]Griffond, J., Casalis, G., and Pineau, J.-P., "Spatial Instability of Flow in a Semiinfinite Cylinder with Fluid Injection through Its Porous Walls," *European Journal of Mechanics B/Fluids,* Vol. 19, No. 1, 2000, pp. 69-87.

[18]Casalis, G., Avalon, G., and Pineau, J.-P., "Spatial Instability of Planar Channel Flow with Fluid Injection through Porous Walls," *The Physics of Fluids,* Vol. 10, No. 10, 1998, pp. 2558-2568.

[19]Griffond, J., and Casalis, G., "On the Nonparallel Stability of the Injection Induced Two-Dimensional Taylor Flow," *The Physics of Fluids,* Vol. 13, No. 6, 2001, pp. 1635-1644.

[20]Féraille, T., Casalis, G., and Dupays, J., "Particle Effects on Solid-Propellant Motors Flow Stability," AIAA Paper 2002-3611, July 2002.

[21]Griffond, J., and Casalis, G., "On the Dependence on the Formulation of Some Nonparallel Stability Approaches Applied to the Taylor Flow," *The Physics of Fluids,* Vol. 12, No. 2, 2000, pp. 466-468.

[22]Ugurtas, B., Avalon, G., Lupoglazoff, N., Vuillot, F., and Casalis, G., "Stability and Acoustic Resonance of Internal Flows Generated by Side Injection," *Solid Propellant Chemistry, Combustion, and Motor Interior Ballistics*, Vol. 185, edited by V. Yang, T. B. Brill, and W.-Z. Ren, AIAA Progress in Astronautics and Aeronautics, Washington, DC, 2000, pp. 823-836.

[23]Majdalani, J., "Physicality of Core Flow Models in Rocket Motors," *Journal of Propulsion and Power,* Vol. 19, No. 1, 2003, pp. 156-159.

[24]Flandro, G. A., "Nonlinear Unsteady Solid Propellant Flame Zone Analysis," AIAA Paper 98-3700, 1998.

[25]Flandro, G. A., and Majdalani, J., "Aeroacoustic Instability in Rockets," *AIAA Journal,* Vol. 41, No. 3, 2003, pp. 485-497.

[26]Flandro, G. A., Fischbach, S. R., Majdalani, J., and French, J. C., "Nonlinear Rocket Motor Stability Prediction: Limit Amplitude, Triggering, and Mean Pressure Shift," AIAA Paper 2004-4054, July 2004.

[27]Majdalani, J., and Vyas, A. B., "Inviscid Models of the Classic Hybrid Rocket," AIAA Paper 2004-3474, July 2004.

[28]Terrill, R. M., and Colgan, T., "Some Simple Analytic Solutions of the Navier-Stokes Equations," *International Journal of Engineering Science,* Vol. 29, No. 1, 1991, pp. 55-68.